Published in final edited form as:
Angew Chem Int Ed Engl. 2020 March 09; 59(11): 4396–4400. doi:10.1002/anie.202000323.

Mixed Metal–Organic Framework with Multiple Binding Sites for Efficient C_2H_2/CO_2 Separation

Junkuo Gao,
Institute of Functional Porous Materials, The Key laboratory of Advanced Textile Materials and Manufacturing Technology of Ministry of Education, School of Materials Science and Engineering, Zhejiang Sci-Tech University, Hangzhou 310018 (China)

Department of Chemistry, University of Texas at San Antonio One UTSA Circle, San Antonio, (USA)

Xuefeng Qian,
Institute of Functional Porous Materials, The Key laboratory of Advanced Textile Materials and Manufacturing Technology of Ministry of Education, School of Materials Science and Engineering, Zhejiang Sci-Tech University, Hangzhou 310018 (China)

Rui-Biao Lin,
Department of Chemistry, University of Texas at San Antonio One UTSA Circle, San Antonio, TX 78249-0698 (USA)

Rajamani Krishna,
Van’t Hoff Institute of Molecular Sciences, University of Amsterdam Science Park 904, 1098 XH Amsterdam (The Netherlands)

Hui Wu,
NIST Center for Neutron Research, National Institute of Standards and Technology, Gaithersburg, MD 20899-6102 (USA)

Wei Zhou,
NIST Center for Neutron Research, National Institute of Standards and Technology, Gaithersburg, MD 20899-6102 (USA)

Banglin Chen
Department of Chemistry, University of Texas at San Antonio One UTSA Circle, San Antonio, TX 78249-0698 (USA)

Abstract

The separation of C_2H_2/CO_2 is particularly challenging owing to their similarities in physical properties and molecular sizes. Reported here is a mixed metal–organic framework (M’MOF), [Fe(pyz)Ni(CN)$_4$] (**FeNi-M’MOF**, pyz=pyrazine), with multiple functional sites and compact one-

---

jkgao@zstu.edu.cn, ruibiao.lin@utsa.edu, wzhou@nist.gov, banglin.chen@utsa.edu.

Conflict of interest
The authors declare no conflict of interest.

Supporting information and the ORCID identification number(s) for the author(s) of this article can be found under: https://doi.org/10.1002/anie.202000323.

dimensional channels of about 4.0 Å for C_2H_2/CO_2 separation. This MOF shows not only a remarkable volumetric C_2H_2 uptake of 133 cm^3cm^{-3}, but also an excellent C_2H_2/CO_2 selectivity of 24 under ambient conditions, resulting in the second highest C_2H_2-capture amount of 4.54 $molL^{-1}$, thus outperforming most previous benchmark materials. The separation performance of this material is driven by **π–π** stacking and multiple intermolecular interactions between C_2H_2 molecules and the binding sites of **FeNi-M'MOF**. This material can be facilely synthesized at room temperature and is water stable, highlighting **FeNi-M'MOF** as a promising material for C_2H_2/CO_2 separation.

Keywords

acetylene; adsorption; gas separation; iron; metal–organic frameworks

---

Metal–organic frameworks (MOFs) have emerged as very promising porous materials for adsorptive gas separation because they integrate the merits of tunable pore sizes and functional pore surfaces that can realize not only a molecular sieving effect, but also preferential gas binding.[1] Many MOFs have been explored for simplifying various gas separation and purification schemes ranging from mature ones, such as carbon dioxide capture (CO_2) from methane and nitrogen, to more challenging olefin/paraffin and alkyne/alkene separations.[2] For C_2H_2 and CO_2 gas molecules, the similarities in physical properties (differ in boiling point by ca. 3% and ca. 6 K) and identical molecular shapes/sizes (3.3 × 3.3 × 5.7 $Å^3$ for C_2H_2, 3.2 × 3.3 × 5.4 $Å^3$ for CO_2), with kinetic diameters of about 3.3 Å, make it very difficult and challenging to realize efficient porous materials for C_2H_2/CO_2 separation under ambient conditions.[3] A few ultra-microporous MOFs featuring bare oxygen or fluorine base sites have been developed to preferentially bind C_2H_2 molecules through hydrogen-bonding interactions or bind CO_2 molecules through electrostatic interactions, showing high C_2H_2/CO_2 selectivity but low C_2H_2 uptake.[4] Another approach is to incorporate strong adsorption binding sites, mainly open metal sites, into MOFs with large pore volumes to boost the uptake capacity of the preferred gas molecules.[5] **UTSA-74** represents a unique example with open metal centers having two accessible sites which can bind two C_2H_2 molecules, but only one CO_2 molecule, differing from its isomer **MOF-74** which adsorbs similar amounts of C_2H_2 and CO_2 under the same conditions.[5c] Though progress has been made over the past several years, the uptake capacity versus selectivity trade-off still poses a daunting challenge for addressing C_2H_2/CO_2 separation.[6]

The vast database of reported MOF structures enables comparative analyses to target potential candidates with dual functionalities, featuring moderate pore volumes and accessible functional sites, to realize both high gas uptake and separation selectivities. Among plentiful ligands, cyanide is a short and highly basic ligand that is feasible to construct robust MOFs with modest pore aperture size, such as Prussian blue and Hofmann-type compounds.[7] For those MOFs with metalloligands, the open metal sites on ligands are accessible for gas molecules, whereas expected narrow pore structures originating from compact ligands enforce additional multiple intermolecular interactions to form, as demonstrated by a series of mixed metal–organic frameworks (M'MOFs).[8] In this regard, a

Hofmann-type MOF [Fe(pyz)Ni(CN)$_4$] (**FeNi-M'MOF**, pyz=pyrazine), discovered in 2001, showing open nickel sites and polarized surfaces as well as compact pore channels of about 4.0 Å, is particularly interesting.[9] The high density of functional sites and ultra-micropore would collaboratively enforce gas separation with high gas uptake and separation selectivities. Herein we investigate the mixed iron/nickel MOF **FeNi-M'MOF** for potential C_2H_2/CO_2 separation. In this MOF, C_2H_2 molecules are found to preferentially bind the organic moieties and open Ni sites through π–π stacking and multiple intermolecular interactions, respectively, whereas CO_2 molecules mainly distribute on the open Ni sites through relatively weak interactions. In this context, **FeNi-M'MOF** shows a very high C_2H_2/CO_2 selectivity of 24 that is superior to the previous top-performing MOFs while retaining a remarkable C_2H_2 uptake capacity of 133 cm^3cm^{-3}, and thus an excellent C_2H_2-capture capacity of 4.54 mol L^{-1} at 298 K and 1 bar for 50:50 C_2H_2/CO_2 separation, which is close to that of the benchmark UTSA-74 and exceeds that of other out-performing MOFs.[5c]

FeNi-M'MOF is a pillared-layer M'MOF, in which the Fe[Ni(CN)$_4$] layer is connected by the pyz pillars. The Ni atoms show square-planar coordination geometry while Fe atoms are octahedrally coordinated. The Ni atoms are coordinated by carbon atoms of four different cyan groups, whereas the Fe atoms are fully coordinated by nitrogen atoms from four different cyan groups and two pyz linkers. Fe[Ni(CN)$_4$] layers are then connected by pyz linkers into a three-dimensional network with one-dimensional channels of about 4.15 × 4.27 or 3.94 × 4.58 Å^2. The open metal site density of **FeNi-M'MOF** is about 9.2 $mmolcm^{-3}$, which is higher than that of most MOFs, as shown in Table S2 (see the Supporting Information).

FeNi-M'MOF was synthesized at room temperature in water and methanol (Figure 1).[10] By adding the solution of $K_2[Ni(CN)_4]$ into the mixed methanol and water solution of Fe^{2+} and pyz, the **FeNi-M'MOF** microcrystalline powders were obtained after stirring for 30 minutes. The powder X-ray diffraction (PXRD) of products indicated that those products have a good crystallinity and match well with the simulated XRD pattern, indicating the purity of **FeNi-M'MOF**. The resultant **FeNi-M'MOF** was further validated by elemental analysis (EA), thermogravimetry analysis (TGA), energy dispersive spectroscopy (EDS), and X-ray photoelectron spectroscopy (XPS) analysis (see the Supporting Information). This MOF also exhibits excellent water stability as shown in Figure S2. After soaking in water for 30 days, the crystallinity of **FeNi-M'MOF** is still retained. The TGA curve indicated that **FeNi-M'MOF** exhibits a considerable thermal stability up to 200°C (see Figure S4). The thermal stability of **FeNi-M'MOF** was also confirmed by variable-temperature PXRD (see Figure S5), indicating that **FeNi-M'MOF** can maintain its crystalline structure up to about 200°C. The fast and facile synthesis method, excellent water stability, and good thermal stability indicate **FeNi-M'MOF** is a promising separation material for scale-up synthesis.

The Brunauer-Emmett-Teller (BET) surface area of **FeNi-M'MOF** was measured to be 383 m^2g^{-1} by an N_2 sorption experiment at 77 K as shown in Figure 2a. The experimental total pore volume is about 0.25 cm^3g^{-1}, and slightly smaller than the theoretical one calculated from the crystal structure (0.30 cm^3g^{-1}), which can be attributed to the insufficient filling of N_2 molecules in the ultramicroporous pore channels.

The C_2H_2 and CO_2 gas adsorption isotherms of **FeNi-M’MOF** were measured at both 273 and 298 K. As shown in Figure 2b, the volumetric C_2H_2 uptake capacity of **FeNi-M’MOF** is 133 cm^3cm^{-3} (4.29 $mmolg^{-1}$) at 1 bar and 298 K, which is higher than those of many other MOFs, such as **DICRO-4-Ni-i** (52 cm^3cm^{-3}),[4e] **ZJU-60a** (96 cm^3cm^{-3}),[11] $Cu[Ni(pdt)_2]$ (108 cm^3cm^{-3}),[6a] **SNNU-45** (113 cm^3cm^{-3}),[6b] **TIFSIX-2-Cu-i** (116 cm^3cm^{-3}),[4f] **PCP-33** (128 cm^3cm^{-3}),[12] and comparable to those of **UTSA-74** (144 cm^3cm^{-3}),[5c] **FJU-90a** (146 cm^3cm^{-3}),[6c] and **Zn-MOF-74** (150 cm^3cm^{-3}).[13] The CO_2 uptake of **FeNi-M’MOF** is 84 cm^3cm^{-3} (2.72 $mmolg^{-1}$) at 1 bar and 298 K. At 1 bar and 273 K, C_2H_2 and CO_2 uptakes of **FeNi-M’MOF** are up to 145 and 102 cm^3cm^{-3} respectively, as shown in Figure S8. Interestingly, the Pt analogue $[Fe(pyz)Pt(CN)_4]$ (**FePt-M’MOF**; see Figures S10–S12) shows much lower uptake capacities for C_2H_2 and CO_2 (100 and 105 cm^3cm^{-3}, respectively), indicating the potential binding contribution of Ni sites in this type of MOF for C_2H_2 molecules. To evaluate the separation performance of this material, ideal adsorbed solution theory (IAST) was employed to calculate the adsorption selectivity. As shown in Figure 2c, at 100 kPa and 298 K, the C_2H_2/CO_2 (50:50) selectivity of **FeNi-M’MOF** is 24. The selectivity of **FeNi-M’MOF** is higher than those of most MOFs, such as **Zn-MOF-74** (1.92),[5c] **FJU-90a** (4.3),[6c] **UTSA-74a** (8.2),[5c] **JCM-1** (13.4),[4b] **DICRO-4-Ni-i** (13.9),[4e] and benchmark **HOF-3a** (21).[14] It should be noted that both the uptake capacity and separation selectivity can significantly affect the practical performance of an adsorbent. **HOF-3a** has a high selectivity, but the low uptake of C_2H_2 reduced its separation performance. In contrast, **FeNi-M’MOF** can address such trade-offs between the adsorption capacity and selectivity as shown in Figure 2d. The high selectivity and high C_2H_2 adsorption capacity of **FeNi-M’MOF** jointly reveal its useful separation potential for C_2H_2/CO_2.

Transient breakthrough simulations were conducted to demonstrate the C_2H_2/CO_2 separation performance of **FeNi-M’MOF**. The simulations in Figure 3a demonstrate the **FeNi-M’MOF** is of potential use for this challenging separation of C_2H_2/CO_2 mixtures. The C_2H_2/CO_2 mixtures (50:50) were used as feeds to mimic the industrial process conditions. Pure CO_2 first eluted through the bed, where the CO_2 purity was 99.95%, followed by the breakthrough of C_2H_2 after a certain time, τ_{break}, during which **FeNi-M’MOF** was saturated by C_2H_2. The C_2H_2-capture amount of **FeNi-M’MOF** is 4.54 $molL^{-1}$ based on the simulated column breakthrough, which is close to that of the benchmark UTSA-74 (4.86 $molL^{-1}$)[5c] and higher than those of most out-performing MOFs, such as **Zn-MOF-74** (4.06 $molL^{-1}$),[5c] **FJU-90a** (4.16 $molL^{-1}$),[6c] and **PCP-33** (4.16 $molL^{-1}$).[12] Accordingly, **FeNi-M’MOF** shows not only a high C_2H_2/CO_2 selectivity and high C_2H_2 uptake but also high C_2H_2-capture capability from gas mixtures, endowing this material with a useful C_2H_2/CO_2 separation potential. Based on experimental breakthrough studies, we further evaluated the performance of **FeNi-M’MOF** in near practical separation processes for a C_2H_2/CO_2 mixture (50:50 v/v) as shown in Figure 3b. Indeed, **FeNi-M’MOF** exhibits excellent C_2H_2/CO_2 mixture separation performance at 298 K. CO_2 was first eluted through the adsorption bed without any detectable C_2H_2, whereas the latter was retained in the MOF column for a remarkable period prior to saturate the MOF. The retention time of pure CO_2 and C_2H_2 for C_2H_2/CO_2 (50:50 v/v) mixture on **FeNi-M’MOF** are up to 24 and 40 min, respectively. Accordingly, the captured C_2H_2 was calculated to be 4.10 molL^{-1} with a separation factor of 1.7.

The isosteric heat of adsorption (Q_{st}) has been used to evaluate the strength of interaction between the adsorbent and the adsorbate, which is calculated (see Figure S13) from the adsorption isotherms at 273 and 298 K. The Q_{st} values are 27–32.8 and about 24.5 kJmol^{-1} of **FeNi-M'MOF** for C_2H_2 and CO_2, respectively. The Q_{st} value of C_2H_2 in **FeNi-M'MOF** is lower than those of other MOFs such as **HKUST-1** (39 kJmol^{-1}),[15] **FeMOF-74** (47.5 kJmol^{-1}),[16] and **SIFSIX-2-Cu-i** (41.9 kJmol^{-1}),[1e] and is comparable to that of **UTSA-74** (31 kJmol^{-1}).[5c] These data indicate **FeNi-M'MOF** has a lower regeneration energy for C_2H_2 production, which would be beneficial for practical applications.

To understand the separation performance of **FeNi-M'MOF**, the adsorption modes of C_2H_2 in **FeNi-M'MOF** were established by DFT-D calculations (see Figure S14). The modeling structures indicated that there are two binding sites for C_2H_2 in **FeNi-M'MOF**: Site I, located in the middle of two adjacent pyz rings, where C_2H_2 was adsorbed through the **π–π** interactions between C_2H_2 and the pyz rings (see Figure S14a). The C_2H_2 static binding energy in site I is up to 41.4 kJmol^{-1}. Site II, located in the middle of two adjacent Ni open metal sites, where C_2H_2 a molecule is adsorbed through the interactions between C≡C and Ni open metal sites and is perpendicular to *c* axis. The C_2H_2 static binding energy in this site is 29.9 kJmol^{-1}, which is smaller than that of site I (see Figure S14b).

Further visualization of these host–guest interactions was carried out through high-resolution neutron powder diffraction experiments. The crystal structure under low C_2D_2 loading was measured first (Figure 4a). As expected, C_2D_2 molecules preferentially distribute on site I. C_2D_2 molecules were identified between the two pyz rings through **π–π** stacking (3.552 Å). The C_2D_2 molecules show a titling angle of 27.4° from the [001] direction (crystallographic *c* axis; see Figure S15a). In addition, multiple intermolecular interactions were also observed between C_2D_2 and **FeNi-M'MOF** ($D^{\delta+}\cdots N^{\delta-}$: 2.977 Å, $C^{\delta-}\cdots N^{\delta-}$: 3.808 Å, Figure 4c; see Figure S15b). In contrast, the preferential CO_2 binding site is located at the open Ni site (Figure 4b). The electronegative $O^{\delta-}$ atoms of CO_2 interact with the positive open-metal site $Ni^{\delta+}$. However, the distance across the channel is insufficient for favorable $Ni^{\delta+}\cdots O^{\delta-}{=}C{=}O^{\delta-}\cdots Ni^{\delta+}$ interactions to form in the structure. Thus, CO_2 molecules were adsorbed near the center of the channel and parallel to the channel. $O^{\delta-}$ atom of CO_2 inserts between the adjacent two $Ni^{\delta+}$ atoms from different layers and the distance of $O^{\delta-}\cdots Ni^{\delta+}$ are 3.746 and 3.325 Å, respectively (Figure 4d). This type interaction is relatively weak, consistent with the gentle adsorption isotherm and low Q_{st} value of CO_2 in **FeNi-M'MOF**. The multiple binding sites of **FeNi-M'MOF** for gas molecules and its different binding modes toward C_2H_2 and CO_2 enable **FeNi-M'MOF** to selectively adsorb C_2H_2 from CO_2 with both high C_2H_2 uptake and remarkable C_2H_2/CO_2 selectivity.

In summary, highly selective C_2H_2/CO_2 separation has been successfully realized by a mixed iron/nickel MOF **FeNi-M'MOF** using a metalloligand approach. The structural features the of cyanonickelate and optimal pore channels in this MOFallow C_2H_2 molecules to interact at multiple binding sites, with both very high C_2H_2 uptake and C_2H_2/CO_2

selectivity in volumetric ratio. The so-called dual functionality in this material enables this MOF to serve as one of the best materials for C_2H_2/CO_2 separation in terms of C_2H_2-capture capability. This work also illustrates an outstanding example to further reveal the huge separation potential of MOF adsorbents, especially for challenging gas separation and purification. The active ongoing research affords tremendous opportunities for energy-efficient separation.

Supplementary Material

Refer to Web version on PubMed Central for supplementary material.

Acknowledgements

This work was supported by the Zhejiang Provincial Natural Science Foundation of China (LY20E020001), National Natural Science Foundation of China (51602301 and 51672251), and the Welch Foundation (AX-1730). J.G. acknowledges the Fundamental Research Funds of Zhejiang Sci-Tech University (2019Q007).

References

[1]. a)Li H, Li L, Lin R-B, Zhou W, Xiang S, Chen B, Zhang Z, EnergyChem 2019, 1, 100006;b)Ding M, Flaig RW, Jiang H-L, Yaghi OM, Chem. Soc. Rev 2019, 48, 2783–2828; [PubMed: 31032507] c)Lin R-B, Li L, Zhou H-L, Wu H, He C, Li S, Krishna R, Li J, Zhou W, Chen B, Nat. Mater 2018, 17, 1128–1133; [PubMed: 30397312] d)Taylor MK, Runčevski T, Oktawiec J, Bachman JE, Siegelman RL, Jiang H, Mason JA, Tarver JD, Long JR, J. Am. Chem. Soc 2018, 140, 10324–10331; [PubMed: 30032596] e)Cui X, Chen K, Xing H, Yang Q, Krishna R, Bao Z, Wu H, Zhou W, Dong X, Han Y, Li B, Ren Q, Zaworotko MJ, Chen B, Science 2016, 353, 141–144; [PubMed: 27198674] f)Cadiau A, Adil K, Bhatt PM, Belmabkhout Y, Eddaoudi M, Science 2016, 353, 137–140; [PubMed: 27387945] g)Lin R-B, Xiang S, Zhou W, Chen B, Chem 2019, 10.1016/j.chempr.2019.1010.1012.

[2]. a)Chen K-J, Madden DG, Mukherjee S, Pham T, Forrest KA, Kumar A, Space B, Kong J, Zhang Q-Y, Zaworotko MJ, Science 2019, 366, 241–246; [PubMed: 31601769] b)Liu Y, Chen Z, Liu G, Belmabkhout Y, Adil K, Eddaoudi M, Koros W, Adv. Mater 2019, 31, 1807513;c)Cui WG, Hu TL, Bu XH, Adv. Mater 2019, 31, 1806445;d)Siegelman RL, Milner PJ, Kim EJ, Weston SC, Long JR, Energy Environ. Sci 2019, 12, 2161–2173; [PubMed: 33312228] e)Li L, Lin R-B, Krishna R, Li H, Xiang S, Wu H, Li J, Zhou W, Chen B, Science 2018, 362, 443–446; [PubMed: 30361370] f)Liao P-Q, Huang N-Y, Zhang W-X, Zhang J-P, Chen X-M, Science 2017, 356, 1193–1196; [PubMed: 28619946] g)Yang S, Ramirez-Cuesta AJ, Newby R, Garcia-Sakai V, Manuel P, Callear SK, Campbell SI, Tang CC, Schröder M, Nat. Chem 2014, 7, 121–129; [PubMed: 25615665] h)Aubrey ML, Kapelewski MT, Melville JF, Oktawiec J, Presti D, Gagliardi L, Long JR, J. Am. Chem. Soc 2019, 141, 5005–5013. [PubMed: 30827099]

[3]. Reid CR, Thomas KM, J. Phys. Chem. B 2001, 105, 10619–10629.

[4]. a)Yang H, Trieu TX, Zhao X, Wang Y, Wang Y, Feng P, Bu X, Angew. Chem. Int. Ed 2019, 58, 11757–11762; Angew. Chem. 2019, 131, 11883–11888;b)Lee J, Chuah CY, Kim J, Kim Y, Ko N, Seo Y, Kim K, Bae TH, Lee E, Angew. Chem. Int. Ed 2018, 57, 7869–7873; Angew. Chem. 2018, 130, 7995–7999;c)Lin R-B, Li L, Wu H, Arman H, Li B, Lin R-G, Zhou W, Chen B, J. Am. Chem. Soc 2017, 139, 8022–8028; [PubMed: 28574717] d)Jiang M, Cui X, Yang L, Yang Q, Zhang Z, Yang Y, Xing H, Chem. Eng. J 2018, 352, 803–810;e)Scott HS, Shivanna M, Bajpai A, Madden DG, Chen K-J, Pham T, Forrest KA, Hogan A, Space B, Perry IV JJ, Zaworotko MJ, ACS Appl. Mater. Interfaces 2017, 9, 33395–33400; [PubMed: 28128918] f)Chen K-J, Scott HS, Madden DG, Pham T, Kumar A, Bajpai A, Lusi M, Forrest KA, Space B, Perry IV JJ, Zaworotko MJ, Chem 2016, 1, 753–765;g)Qazvini OT, Babarao R, Shi Z-L, Zhang Y-B, Telfer SG, J. Am. Chem. Soc 2019, 141, 5014–5020. [PubMed: 30860821]

[5]. a)Zeng H, Xie M, Huang Y-L, Zhao Y, Xie X-J, Bai J-P, Wan M-Y, Krishna R, Lu W, Li D, Angew. Chem. Int. Ed 2019, 58, 8515–8519; Angew. Chem. 2019, 131, 8603–8607;b)Duan J,

Higuchi M, Zheng J, Noro S-I, Chang I-Y, Hyeon-Deuk K, Mathew S, Kusaka S, Sivaniah E, Matsuda R, J. Am. Chem. Soc 2017, 139, 11576–11583; [PubMed: 28747050] c)Luo F, Yan C, Dang L, Krishna R, Zhou W, Wu H, Dong X, Han Y, Hu T-L, OKeeffe M, Wang L, Luo M, Lin R-B, Chen B, J. Am. Chem. Soc 2016, 138, 5678–5684. [PubMed: 27113684]

[6]. a)Peng Y-L, Pham T, Li P, Wang T, Chen Y, Chen K-J, Forrest KA, Space B, Cheng P, Zaworotko MJ, Zhang Z, Angew. Chem. Int. Ed 2018, 57, 10971–10975; Angew. Chem. 2018, 130, 11137–11141;b)Li Y-P, Wang Y, Xue Y-Y, Li H-P, Zhai Q-G, Li S-N, Jiang Y-C, Hu M-C, Bu X, Angew. Chem. Int. Ed 2019, 58, 13590–13595; Angew. Chem. 2019, 131, 13724–13729;c)Ye Y, Ma Z, Lin R-B, Krishna R, Zhou W, Lin Q, Zhang Z, Xiang S, Chen B, J. Am. Chem. Soc 2019, 141, 4130–4136. [PubMed: 30793890]

[7]. a)Aguilà D, Prado Y, Koumousi ES, Mathoniere C, Clérac R, Chem. Soc. Rev 2016, 45, 203–224; [PubMed: 26553752] b)Zakaria MB, Chikyow T, Coord. Chem. Rev 2017, 352, 328–345;c)Otsubo K, Haraguchi T, Kitagawa H, Coord. Chem. Rev 2017, 346, 123–138;d)Sakaida S, Otsubo K, Sakata O, Song C, Fujiwara A, Takata M, Kitagawa H, Nat. Chem 2016, 8, 377–383; [PubMed: 27001734] e)Deshmukh MM, Ohba M, Kitagawa S, Sakaki S, J. Am. Chem. Soc 2013, 135, 4840–4849; [PubMed: 23437824] f)Culp JT, Smith MR, Bittner E, Bockrath B, J. Am. Chem. Soc 2008, 130, 12427–12434. [PubMed: 18717562]

[8]. a)Das MC, Xiang S, Zhang Z, Chen B, Angew. Chem. Int. Ed 2011, 50, 10510–10520; Angew. Chem. 2011, 123, 10696–10707;b)Xiang S-C, Zhang Z, Zhao C-G, Hong K, Zhao X, Ding D-R, Xie M-H, Wu C-D, Das MC, Gill R, Tomas K, Chen B, Nat. Commun 2011, 2, 204. [PubMed: 21343922]

[9]. Niel V, Martinez-Agudo JM, Muñoz MC, Gaspar AB, Real JA, Inorg. Chem 2001, 40, 3838–3839. [PubMed: 11466039]

[10]. Gao J, Cong J, Wu Y, Sun L, Yao J, Chen B, ACS Appl. Energy Mater 2018, 1, 5140–5144.

[11]. Duan X, Zhang Q, Cai J, Yang Y, Cui Y, He Y, Wu C, Krishna R, Chen B, Qian G, J. Mater. Chem. A 2014, 2, 2628–2633.

[12]. Duan J, Jin W, Krishna R, Inorg. Chem 2015, 54, 4279–4284. [PubMed: 25884592]

[13]. Xiang S, Zhou W, Zhang Z, Green MA, Liu Y, Chen B, Angew. Chem. Int. Ed 2010, 49, 4615–4618; Angew. Chem. 2010, 122, 4719–4722.

[14]. Li P, He Y, Zhao Y, Weng L, Wang H, Krishna R, Wu H, Zhou W, O'Keeffe M, Han Y, Chen B, Angew. Chem. Int. Ed 2015, 54, 574–577; Angew. Chem. 2015, 127, 584–587.

[15]. He Y, Krishna R, Chen B, Energy Environ. Sci 2012, 5, 9107–9120.

[16]. Bloch ED, Queen WL, Krishna R, Zadrozny JM, Brown CM, Long JR, Science 2012, 335, 1606–1610. [PubMed: 22461607]

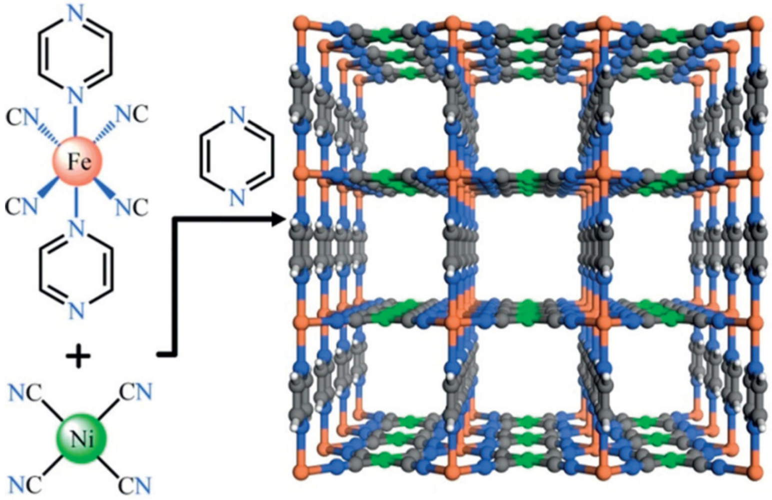

Figure 1.

The crystal structure of **FeNi-M'MOF** viewed along the *a/b* axis. Fe, Ni, C, N, and H in **FeNi-M'MOF** are represented by orange, green, gray, blue, and white, respectively.

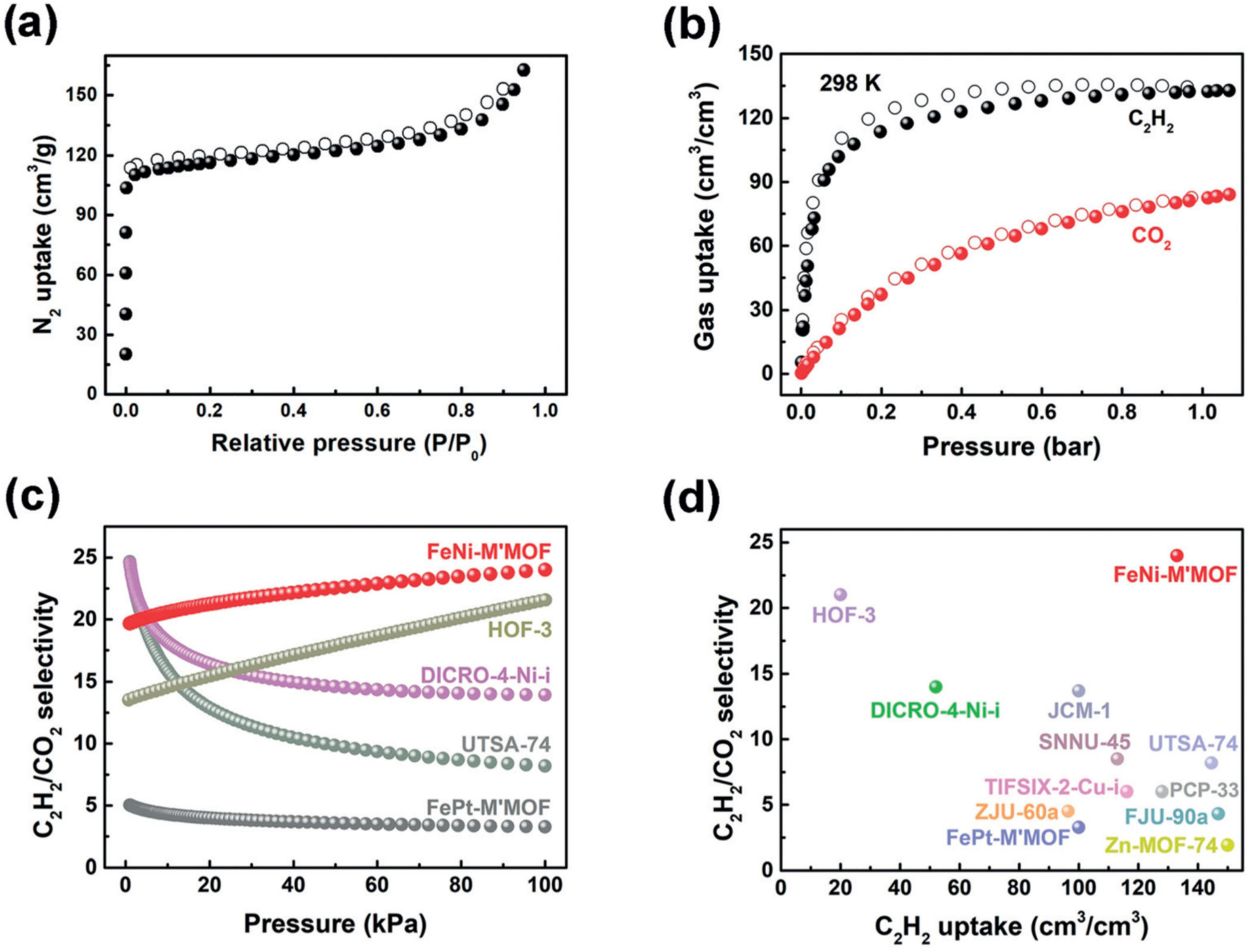

Figure 2.

a) N_2 sorption isotherms for **FeNi-M’MOF** at 77 K. b) C_2H_2 and CO_2 sorption isotherms for **FeNi-M’MOF** at 298 K. c) Comparison of IAST selectivities for equimolar C_2H_2/CO_2 mixtures in **FeNi-M’MOF, FePt-M’MOF** and other materials in the range of 0–1 bar at 298 K. d) Comparison of C_2H_2/CO_2 adsorption selectivity and volumetric C_2H_2 uptake at 1 bar in **FeNi-M’MOF, FePt-M’MOF** and other porous materials.

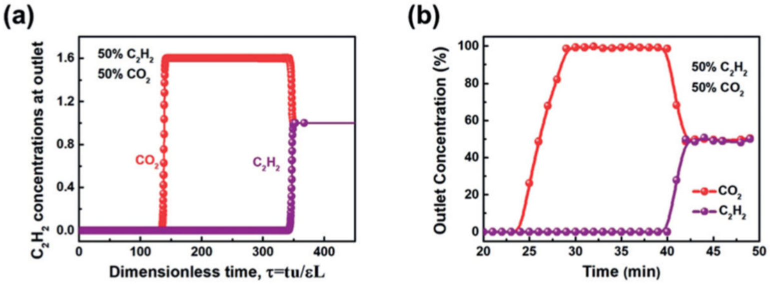

Figure 3.

a) Transient breakthrough simulations for separation of equimolar C_2H_2/CO_2 mixture using **FeNi-M'MOF** at 298 K, with a partial pressure of 50 kPa for each. b) Experiment breakthrough curves for equimolar C_2H_2/CO_2 mixture in a packed column with **FeNi-M'MOF** at 298 K and 1 bar.

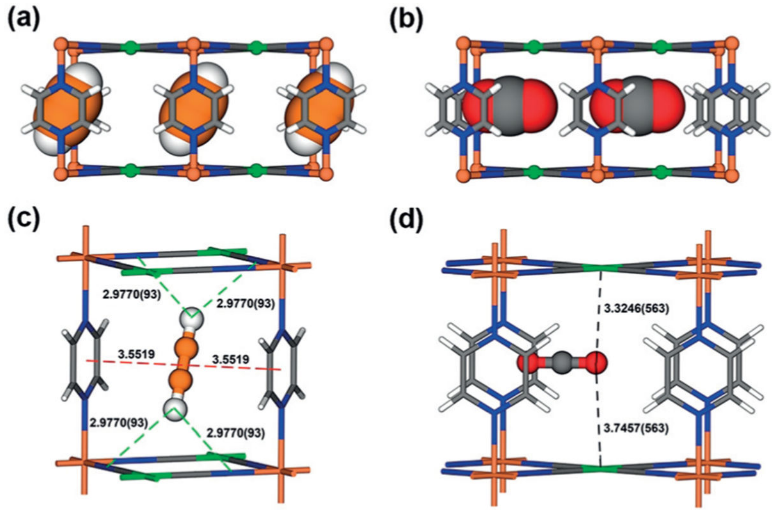

Figure 4.

Neutron diffraction crystal structure of a) **FeNi-M’MOF$\supset C_2D_2$** and b) **FeNi-M’MOF$\supset CO_2$**, viewed from the *a/b* axis. Adsorption binding sites of c) C_2D_2 and c) CO_2 for **FeNi-M’MOF**. Fe, Ni, C, N, O, H in **FeNi-M’MOF** and CO_2 are represented by orange, green, gray, blue, red, and white, respectively; C and D in C_2D_2 are represented by orange and white, respectively. The labelled distance is measured in Å.